# Laser-Enabled Auger Decay in Rare-Gas Atoms

P. Ranitovic,[1,*] X. M. Tong,[2,3,†] C. W. Hogle,[1] X. Zhou,[1] Y. Liu,[4] N. Toshima,[2] M. M. Murnane,[1] and H. C. Kapteyn[1]

[1]*JILA and Department of Physics, University of Colorado and NIST, Boulder, Colorado 80309-0440, USA*
[2]*Institute of Materials Science, Graduate School of Pure and Applied Sciences, University of Tsukuba,*
*1-1-1 Tennodai, Tsukuba, Ibaraki 305-8573, Japan*
[3]*Center for Computational Sciences, University of Tsukuba, 1-1-1 Tennodai, Tsukuba, Ibaraki 305-8577, Japan*
[4]*College of Engineering, University of California at Berkeley, California 94720, USA*

In rare-gas atoms, Auger decay in which an inner-valence shell $ns$ hole is filled is not energetically allowed. However, in the presence of a strong laser field, a new laser-enabled Auger decay channel can open up to increase the double-ionization yield. This process is efficient at high laser intensities, where an $ns$ hole can be filled within a few femtoseconds of its creation. This novel laser-enabled Auger decay process is of fundamental importance for controlling electron dynamics in atoms, molecules, and materials.

Auger decay is an important decay process in highly excited systems, that is, relevant to radiation physics, x-ray spectroscopy, x-ray lasers, and atmospheric chemistry. In Auger decay, absorption of a high-energy photon leads to the ejection of an inner-shell primary photoelectron. The resulting hole is then filled by an electron from an outer shell, with any excess energy carried away by ejecting a second Auger electron.

Advances in laser and x-ray technology now make it possible to create an inner-shell core hole using a femtosecond or attosecond burst of x rays and to observe or manipulate the resultant photoelectron or Auger electron using an ultrafast infrared (IR) laser. Laser-assisted photoemission was first observed in atoms and more recently in solids [1,2]. It is now used worldwide to characterize x-ray pulses and to capture fast electron dynamics in atoms and materials [3,4]. In a laser-assisted process, an atom or material is simultaneously irradiated by ultrafast x-ray and laser pulses. Characteristic sidebands appear surrounding the photoemission and Auger peaks, corresponding to simultaneous absorption and emission of laser photons in addition to the x-ray photon. The magnitude and shape of these sidebands change as the time delay between the x-ray and laser pulses is changed, encoding information about the x-ray pulse duration as well as any underlying electron dynamics in the atom or material [5–9]. However, to date laser-assisted Auger decay represented a means by which an existing Auger decay channel could be modified and exploited. It was not understood that a strong laser field can also turn on and control the Auger decay process itself—which is a fundamental decay mechanism for matter exposed to ionizing radiation.

In this Letter we identify through theory and experiment a novel ionization channel that opens up only in the presence of an intense laser field. Experimentally we find that in the presence of a sufficiently intense IR laser and an extreme ultraviolet (XUV) field, the double-ionization yield of Ar is enhanced by 50% compared to the case when the laser pulse arrives after the XUV pulse. Although $Ar^{2+}$ can also be produced by sequential and nonsequential absorption of XUV and IR photons (shake-up and shake-off processes), the observed ratio of doubly to singly ionized argon is larger than can be theoretically explained by these processes alone. Therefore, we need to include a new double-ionization pathway: IR laser-enabled Auger decay (LEAD), which is energetically forbidden without the presence of the IR field. Normally in a rare-gas atom, Auger decay following the creation of an $ns$ hole by an XUV photon is not energetically allowed. However, our theoretical predictions show that the laser-enabled Auger decay rates are even larger than the radiative decay rates for laser intensities above $10^{13}$ W/cm$^2$, and thus the inner-valence hole can be filled by the LEAD process on few-femtosecond time scales. This novel decay channel is also quite general, representing a fundamentally new mechanism for generating ions and Auger electrons that must be considered in ultrafast x-ray experiments. It also provides a new route for controlling electron dynamics using ultrafast light fields.

Our experimental setup consists of a high-power (30 W), high repetition rate (10 kHz) 40 fs Ti:sapphire laser system coupled to a COLTRIMS apparatus. Using part of the laser output, high harmonics are generated in Ar gas and then refocused into a separate Ar gas target in the COLTRIMS chamber using a pair of multilayer XUV optics centered at 42 eV. The remaining laser beam is temporally and spatially recombined with the XUV beam in a collinear fashion, and focused onto the target jet at a peak intensity of $10^{13}$ W/cm$^2$. Low-order harmonics, up to the 13th order, are also reflected by our multilayer optics (reflectivity $\approx 5\%$). Because of a higher photoionization cross section at $\approx 20$ eV, the $Ar^+$ yield from these lower energy photons
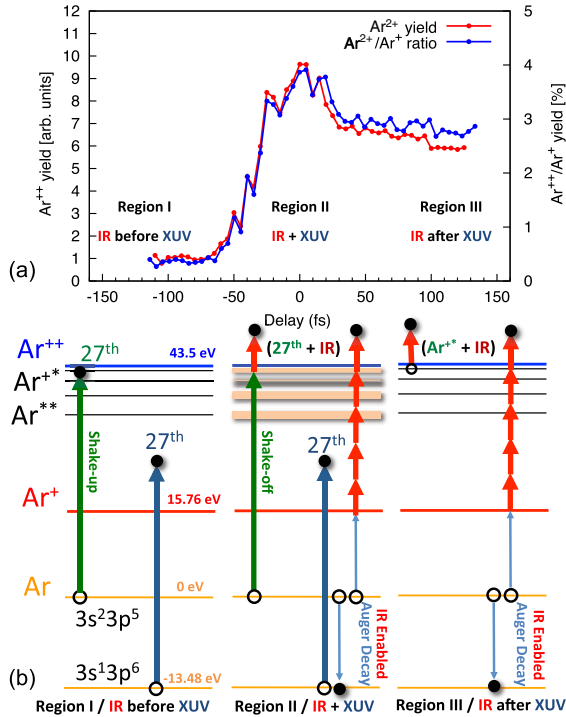
FIG. 1 (color online). (a) $Ar^{2+}$ and $Ar^{2+}/Ar^+$ yields as a function of the XUV pump and IR probe delay. The three regions correspond to the different relative delays of the XUV and IR pulses. (b) Schematic diagram of double-ionization pathways in different regions. In region II, the main double-ionization channels are labeled as shake-off and IR-enabled Auger decay. In region I, since Auger decay is not energetically allowed, the XUV pulse creates $Ar^{+*}$ and $Ar^{**}$ states. These states, respectively, radiatively decay and autoionize, and do not contribute to the $Ar^{2+}$ yield. In region III the IR pulse arrives after the XUV pulse, and doubly ionizes the $Ar^{+*}$ and $Ar^{**}$ states created by the XUV pulse, and opens up the LEAD channel. In region II the IR field enhances the $Ar^{2+}$ yield by altering the atom's electronic structure, influencing thus the LEAD, shake-up or shake-off, and other allowed channels.

dominates our signal. However, the COLTRIMS technique allows us to observe singly and doubly charged ions in coincidence with electrons, allowing us to distinguish the $Ar^+$ yield originating from different ionization channels.

Figure 1(b) illustrates the possible single- and double-ionization channels in Ar. We consider three cases: the IR pulse precedes the XUV pulse (region I); the two pulses overlap in time (region II); and the IR pulse follows the XUV pulse (region III). Figure 1(a) shows that the $Ar^{2+}$ yield is negligible for region I, while the yield increases dramatically for positive time delays, peaking in region II when the XUV and IR pulses overlap. The enhancement of the $Ar^{2+}$ yield in region III is due to field ionization of $Ar^{+*}$ and $Ar^{**}$ states excited by the XUV pulse, and due to the LEAD process. We note that without the IR pulse the $3p^{-1}$ and $3s^{-1}$ highly-excited $Ar^+$ states radiatively decay on a nanosecond time-scale. The most interesting behavior, however, occurs in region II when the XUV and laser pulses

overlap in time. The observed enhancement in the $Ar^{2+}$ signal strongly suggests that the laser field modifies the mechanism for populating the $Ar^{+*}/Ar^{**}$ states created after the absorption of a single XUV photon. There are two possible mechanisms for the observed enhanced $Ar^{2+}$ yield in region II: first, the laser field can influence the shake-up and IR-ionization sequence by modifying, broadening, and shifting of the $Ar^{+*}$ resonances [10,11]; and second, the laser field can provide the additional energy required to open up a shake-off channel, which does not occur in region III (where the XUV pulse excites unperturbed $Ar^{+*}$ states that are sequentially ionized by the IR pulse).

To investigate the physical origin of the $Ar^{2+}$ signal we note that there are four possible ways to create $Ar^{2+}$ in the presence of simultaneous IR and XUV (42 eV) fields: (a) IR assisted shake-off and shake-up processes in regions II and III, (b) knockout ionization processes, (c) single-photon double excitation by the XUV pulse, followed by IR-induced double-ionization, and (d) a new mechanism of IR-enabled Auger decay of an XUV-induced $3s$ hole.

The double-ionization probability of Ar through channels (a) and (b) depends on the excess energy available above the double-ionization threshold of 43.5 eV in Ar [12]. Field ionization by the IR field provides this excess energy when Ar is exposed to a combined action of XUV and IR fields. Thus, to estimate the expected $Ar^{2+}/Ar^+$ ratio from channels (a) and (b), we first calculate the photoelectron yields above and below the double-ionization threshold. Second, we calculate the shake-up and shake-off ionization probabilities from the $3s$ and $3p$ orbitals. We do this by solving the time-dependent Schrödinger integral equation [13] by the split-operator method in the energy representation [14] to obtain the above-threshold ionization (ATI) distribution $dP(E)/dE$ from both $3s$ and $3p$ orbitals. The IR intensity used in the calculation was $5 \times 10^{12}$ W/cm$^2$. The detailed numerical method can be found elsewhere [15]. The double-ionization yield depends on the ATI spectra with total energy higher than the double-ionization threshold, according to

$$P^{++} = \int_{E>E_c} \frac{dP(E)}{dE} dE, \qquad (1)$$

where $E$ is the ATI electron energy and $E_c$ is the minimum energy needed to open the double-ionization channel. We find that the ATI electrons above the $E_c$ threshold contain 30% of the total ATI yield. On the other hand, the total shake-off (including shake-up) probability after removing a $3p$ or $3s$ electron can be calculated by using the sudden approximation

$$P = (1 - \langle \tilde{\psi}_{3p} | \psi_{3p} \rangle^2) n_{occ}, \qquad (2)$$

where $\tilde{\psi}_{3p}$ and $\psi_{3p}$ are the $3p$ wave functions of Ar and $Ar^+$ calculated by utilizing density functional theory with

the self-interaction correction method [16], while $n_{occ}$ is the number of the valence Ar$^+$ electrons. We find the shake-up or shake-off probability to be $P = 4\%$, after the sudden removal of $3p$ and $3s$ electrons. By multiplying this probability with the double-ionization photoelectron yield calculated above, we find that the upper limit for the shake-off yield is 1.2%. However, the measured fractional Ar$^{2+}$ yield shown in Fig. 1(a) peaks at 4% near time zero, which means that channels (c) and (d) must also contribute significantly to double ionization.

In the case of process (c)—single-photon double excitation to Ar$^{**}$ by the XUV pulse followed by IR-induced double ionization—the first step of creating Ar$^{**}$ has been studied using synchrotron light in the energy range considered here [17,18]. In the presence of an additional IR field, the XUV-induced Ar$^{**}$ states can be promoted into the double-ionization continuum, thus contributing to the total Ar$^{2+}$ yield. Because doubly excited states in general autoionize on femtosecond time scales, their signature would be seen as a decay in the Ar$^{2+}$ yield at long time delays, as indeed seen in region III of Fig. 1(a). Calculating exactly how the IR laser influences the creation of doubly excited states in region II still remains a theoretical challenge.

Route (d), which represents a novel IR-enabled Auger decay route for the XUV-induced $3s$ hole [Fig. 1(b)], is also possible. After the creation of a $3s$ hole with the XUV pulse, the $3p$-$3s$ Auger decay is energetically forbidden. However, this double-ionization channel can be opened up in the presence of a sufficiently high IR laser field. In the case of Ar, an Auger-induced $3p$ electron needs 14.8 eV of extra energy to reach the double-ionization continuum. Assuming that the wave functions of the atomic ion with a subshell hole ($N-1$ electron system), the doubly ionized ion core ($N-2$ electron system), and the Auger electron are $\Psi_h(N-1)$, $\Psi_c(N-2)$, and $\psi_a$ with the corresponding Hamiltonians $H_h(N-1)$, $H_c(N-2)$, and $h_a$, respectively, we can write the time evolution of the Auger electron wave function as

$$\psi_a(\mathbf{r}, t) = -i \int_{-\infty}^{t} e^{-i \int_{\tau}^{t} h_a(t')dt'} e^{-i(E_h - E_c)\tau} F(\mathbf{r}) d\tau. \quad (3)$$

Here $E_h$ and $E_c$ are the total energies of the $\Psi_h(N-1)$ and $\Psi_c(N-2)$ states, respectively. To derive the above equation, we assume that the IR laser only affects the Auger electron and that it does not perturb the occupied orbitals in $\Psi_h(N-1)$ and $\Psi_c(N-2)$. Since the Auger process is a two-electron process, $F(\mathbf{r})$ is evaluated as

$$F(\mathbf{r}) = \sum_{i=1}^{N-2} \left\langle \Psi_c(N-2) \left| \frac{1}{|\mathbf{r} - \mathbf{r}_i|} \right| \Psi_h(N-1) \right\rangle, \quad (4)$$

which does not depend on the IR field. The Hamiltonian of the Auger electron in the IR laser is written as

$$h_a(t) = -\frac{\nabla^2}{2} + V_{\text{eff}}(r) - zE(t), \quad (5)$$

where $V_{\text{eff}}(r)$ is the model potential [19] of the atomic ions, $z$ is the electron coordinate along the IR polarization direction, and $E(t)$ is the IR field strength. For Ar, $|\Psi_h(N-1)\rangle$ can be written as $|3s3p^{6\,2}S\rangle$, which can be represented as [20]

$$|\Psi_h(N-1)\rangle = \frac{1}{\sqrt{15}} |3s(3p^{4\,1}S)3p^{2\,2}S\rangle$$
$$+ \frac{1}{\sqrt{3}} |3s(3p^{4\,1}D)3p^{2\,2}S\rangle$$
$$+ \sqrt{\frac{3}{5}} |3s(3p^{4\,3}P)3p^{2\,2}S\rangle. \quad (6)$$

$|\Psi_c(N-2)\rangle$ is $|3s^2 3p^{4\,1}S\rangle$ or $|3s^2 3p^{4\,1}D\rangle$. The last term in Eq. (6) does not contribute to the LEAD due to conservation of the angular momentum and parity. The final doubly charged ions created by the LEAD can be in the $^1S$ (the upper limit is $1/15$) or $^1D$ (the upper limit is $1/3$) states, limiting the total double-ionization yield to be 40% of the hole population.

By defining a radial function $f(r)$ as

$$f(r) = \int_0^\infty R_{3s}(r_1) \frac{r_<}{r_>^2} R_{3p}(r_1) R_{3p}(r) r_1^2 dr_1, \quad (7)$$

where $r_<$ ($r_>$) is the smaller (larger) one of the $r$ and $r_1$, and $R_{3s}$ and $R_{3p}$ being the radial wave functions of $3s$ and $3p$ states, we obtain

$$F(\mathbf{r}) = \begin{cases} -\frac{1}{\sqrt{3}} f(r) Y_{00}(\hat{\mathbf{r}}) & \text{for } ^1S, \\ -\sqrt{\frac{2}{15}} f(r) Y_{2M}(\hat{\mathbf{r}}) & \text{for } ^1D. \end{cases} \quad (8)$$

$^1S$ ($^1D$) stands for the final state of the doubly ionized species. Using the expression for $F(\mathbf{r})$, we calculate the Auger election wave function from Eq. (3) numerically [14]. Again, the single electron wave functions of the occupied orbitals in $|\Psi_h(N-1)\rangle$ and $|\Psi_c(N-2)\rangle$ are calculated from the density functional theory with the self-interaction correction method [16].

To speed the convergence of the simulation, we add a temporal window function $e^{-\tau^2/T^2}$ in Eq. (3). Thus, after a long propagation time we can expand $\psi_a$ as

$$\psi_a(\mathbf{r}, t \to \infty) = \int C(\epsilon) \psi_\epsilon(\mathbf{r}) d\epsilon, \quad (9)$$

where $\psi_\epsilon(\mathbf{r})$ is the laser-field-free atomic continuum wave function, and $\epsilon$ is the electron energy [13]. The energy distribution of the emitted electron can be expressed as

$$\frac{dP(\epsilon)}{d\epsilon} = |C(\epsilon)|^2, \quad (10)$$
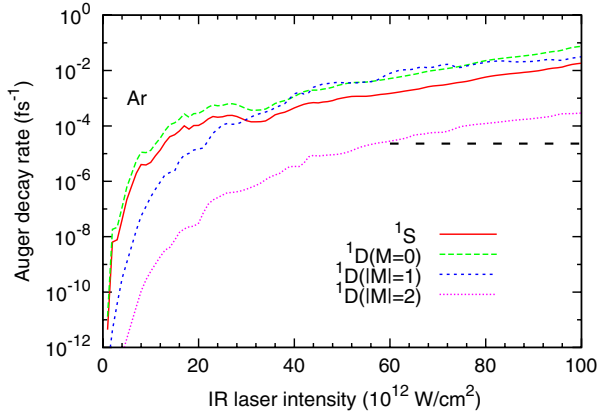
and the LEAD rate can be written as

FIG. 2 (color online). Calculated IR laser-enabled Auger decay rates for Ar. At lower laser intensities, the leading decay channels are the $^1S$ and $^1D(M = 0)$ states. As the IR laser intensity increases, the contribution from the $^1D(M = 0)$ state is larger than that from the $^1S$ state. Radiative $3p$-$3s$ decay is represented by the dashed line.

$$R_a = \frac{\sqrt{2\pi}}{T} \int_0^\infty \frac{dP(\epsilon)}{d\epsilon} \, d\epsilon. \qquad (11)$$

The $\sqrt{2\pi}/T$ term is introduced because we added a temporal window function. If there is no IR laser field present, Eq. (11) reduces to the standard expression for the Auger decay rate. Because of the energy deficiency, the Auger decay rate goes to zero for an inner-valence $3s$ vacancy of Ar without the presence of the IR field.

Based on the above approach, we can now calculate the LEAD rate in Ar. From Fig. 2 we see that laser intensities of $\approx 10^{13}$ W/cm$^2$ can indeed open up a new laser-enabled Auger decay channel, with a rate of $4.3 \times 10^{-4}$ fs$^{-1}$—which is comparable or even larger than the radiative decay rate of the $3p$ electron. Thus, the contribution to the Ar$^{2+}$ yield from the LEAD channel is comparable to contributions from the shake-off channel, and must therefore contribute to the total Ar$^{2+}$ yield.

In conclusion, new ionization pathways are possible when matter is irradiated by intense laser and x-ray fields. In this work, to explain the yield of Ar$^{2+}$ ions in the presence of combined IR and XUV fields, we needed to include a new double-ionization pathway: IR laser-enabled Auger decay, which is energetically forbidden without the presence of the IR field. Our theoretical predictions showed that LEAD rates are even larger than the radiative decay rates for laser intensities above $10^{13}$ W/cm$^2$, and that the $3s$ hole can be filled by the LEAD process on few-femtosecond time scales. This novel decay channel is also quite general, representing a fundamentally new mechanism for generating doubly charged ion cores, ionic Rydberg states, and Auger electrons. It also provides a new scheme for controlling electron dynamics in atoms, molecules, and solids using IR fields.

*predragr@jila.colorado.edu
†tong@ims.tsukuba.ac.jp
[1] J. M. Schins, P. Breger, P. Agostini, R. C. Constantinescu, H. G. Muller, G. Grillon, A. Antonetti, and A. Mysyrowicz, Phys. Rev. Lett. **73**, 2180 (1994).
[2] L. Miaja-Avila and C. Lei et al., Phys. Rev. Lett. **97**, 113604 (2006).
[3] M. Drescher and M. Hentschel et al., Nature (London) **419**, 803 (2002).
[4] L. Miaja-Avila, G. Saatho, S. Mathias, J. Yin, C. L-o-vorakiat, M. Bauer, M. Aeschlimann, M. M. Murnane, and H. C. Kapteyn, Phys. Rev. Lett. **101**, 046101 (2008).
[5] T. Mercouris, Y. Komninos, and C. A. Nicolaides, Phys. Rev. A **76**, 033417 (2007).
[6] C. H. Zhang and U. Thumm, Phys. Rev. A **80**, 032902 (2009).
[7] C. Buth and K. J. Schafer, Phys. Rev. A **80**, 033410 (2009).
[8] Y.-C. Chiang, P. V. Demekhin, A. I. Kule, S. Scheit, and L. S. Cederbaum, Phys. Rev. A **81**, 032511 (2010).
[9] T. Shimizu, T. Sekikawa, T. Kanai, S. Watanabe, and M. Itoh, Phys. Rev. Lett. **91**, 017401 (2003).
[10] P. Ranitovic, X. M. Tong, B. Gramkow, S. De, B. De-Paola, K. P. Singh, W. Cao, M. Magrakvelidze, D. Ray, I. Bocharova, H. Mashiko, A. Sandhu, E. Gagnon, M. M. Murnane, H. Kapteyn, I. Litvinyuk, and C. L. Cocke, New J. Phys. **12**, 013008 (2010).
[11] X. M. Tong and N. Toshima, Phys. Rev. A **81**, 063403 (2010).
[12] J. A. R. Samson, Phys. Rev. Lett. **65**, 2861 (1990).
[13] X. M. Tong, K. Hino, and N. Toshima, Phys. Rev. A **74**, 031405 (2006).
[14] X. M. Tong and S. I. Chu, Chem. Phys. **217**, 119 (1997).
[15] X.-M. Tong and N. Toshima, Phys. Rev. A **81**, 043429 (2010).
[16] X.-M. Tong and S. Chu, Phys. Rev. A **55**, 3406 (1997).
[17] R. P. Madden, D. L. Ederer, and K. Codling, Phys. Rev. **177**, 136 (1969).
[18] K. H. Schartner, B. Mobus, P. Lenz, H. Schmoranzer, and M. Wildberger, Phys. Rev. Lett. **61**, 2744 (1988).
[19] X. Tong and C. Lin, J. Phys. B **38**, 2593 (2005).
[20] R. D. Cowan, The Theory of Atomic Structure and Spectra (University of California, Berkeley, 1981).